Eugster, P., Thiede, R. C., Scherler, D., Stübner, K., Sobel, E. R., Strecker, M. R. (2018): Segmentation of the Main Himalayan Thrust Revealed by Low-Temperature Thermochronometry in the Western Indian Himalaya. - *Tectonics*, *37*, 8, pp. 2710—2726.

DOI: http://doi.org/10.1029/2017TC004752

Tectonics

RESEARCH ARTICLE
10.1029/2017TC004752

Key Points:
- Along and across-strike gradients in apatite fission track (AFT) cooling ages in the western Indian Himalaya document regional change in tectonic style
- Central Himalayan belt of rapid exhumation terminates in the Beas-Lahul area
- No evidence for Lesser Himalayan duplex formation in the Western Himalaya

Supporting Information:
- Supporting Information S1

Correspondence to:
R. C. Thiede,
rasmus.thiede@ifg.uni-kiel.de

Citation:
Eugster, P., Thiede, R. C., Scherler, D., Stübner, K., Sobel, E. R., & Strecker, M. R. (2018). Segmentation of the Main Himalayan Thrust revealed by low-temperature thermochronometry in the western Indian Himalaya. *Tectonics*, *37*, 2710–2726. https://doi.org/10.1029/2017TC004752

Received 3 AUG 2017
Accepted 19 JUL 2018
Accepted article online 30 JUL 2018
Published online 23 AUG 2018

Segmentation of the Main Himalayan Thrust Revealed by Low-Temperature Thermochronometry in the Western Indian Himalaya

Patricia Eugster[1], Rasmus C. Thiede[1,2], Dirk Scherler[3,4], Konstanze Stübner[1], Edward R. Sobel[1], and Manfred R. Strecker[1]

[1]Institute of Earth and Environmental Science, University of Potsdam, Potsdam, Germany, [2]Now at Institute of Geosciences Christian Albrecht, Universität zu Kiel, Kiel, Germany, [3]Earth Surface Geochemistry, GFZ German Research Centre for Geosciences, Potsdam, Germany, [4]Institute of Geological Sciences, Freie Universität Berlin, Berlin, Germany

Abstract Despite remarkable tectonostratigraphic similarities along the Himalayan arc, pronounced topographic and exhumational variability exists in different morphotectonic segments. The processes responsible for this segmentation are debated. Of particular interest is a 30- to 40-km-wide orogen-parallel belt of rapid exhumation that extends from central Nepal to the western Himalaya and its possible linkage to a midcrustal ramp in the basal décollement, and the related growth of Lesser Himalayan duplex structures. Here we present 26 new apatite fission track cooling ages from the Beas-Lahul region, at the transition from the Central to the Western Himalaya (~77°–78°E) to investigate segmentation in the Himalayan arc from a thermochronologic perspective. Together with previously published data from this part of the orogen, we document significant lateral changes in exhumation between the Dhauladar Range to the west, the Beas-Lahul region, and the Sutlej area to the east of the study area. In contrast to the Himalayan front farther east, exhumation in the far western sectors is focused at the frontal parts of the mountain range and associated with the hanging wall of the Main Boundary Thrust fault ramp. Our results allow us to spatially correlate the termination of the rapid exhumation belt with a midcrustal ramp to the west. We suggest that a plunging anticline at the northwestern edge of the Larji-Kullu-Rampur window represents the termination of the Central Himalayan segment, which is related to the evolution of the Lesser Himalayan duplex.

1. Introduction

Since the onset of the India-Eurasia collision ~54 Ma ago, India has been moving northward relative to Tibet resulting in the growth of the Himalayan orogenic wedge, Tibet's southern plateau margin. The Himalaya is commonly described as cylindrical-shaped orogen with major along-strike tectono-stratigraphic similarities (Figure 1); this includes the lithologies and structures of the Lesser and Higher Himalaya, the southward directed growth of the Lesser Himalayan duplex structures, and approximately synchronous deformation along major structural boundaries. These include the Southern Tibetan Detachment (STD), the Main Central Thrust (MCT), the Main Boundary Thrust (MBT), and the Main Frontal Thrust (MFT; Bendick & Bilham, 2001; Burg et al., 1984; DeCelles et al., 2016; Gansser, 1964; Hodges, 2000; Kohn, 2014; Schelling & Arita, 1991; Srivastava & Mitra, 1994; Valdiya, 1980). Despite many regional similarities, the orogen is characterized by significant lateral variations regarding the role of major structures (Yin, 2006), topography (Bookhagen & Burbank, 2006; Duncan et al., 2003), and exhumation rates (Harvey et al., 2015; Robert et al., 2011; Thiede et al., 2009; Thiede & Ehlers, 2013; van der Beek et al., 2016). In particular, segments of the belt that are characterized by a pronounced topographic step between Lesser and Higher Himalaya are associated with a focused exhumation; they alternate with segments where topographic steps or major tectono-stratigraphic units are missing and exhumation rates are lower (Duncan et al., 2003; Robert et al., 2011; Thiede et al., 2017). The potential structural and tectonic controls that determine these spatially variable topographic, deformation, and exhumation patterns have remained controversial.

One of the structurally most prominent segments of the orogen is the Central Himalaya, a region extending from central Nepal to Garhwal (77°E–91°E; e.g., Hodges, 2000); this sector of the range has been at the center of discussions about the structural architecture and evolution of the entire mountain belt (e.g., Avouac, 2003; Gansser, 1964; Hodges, 2000; Kohn, 2014; Robinson et al., 2001).

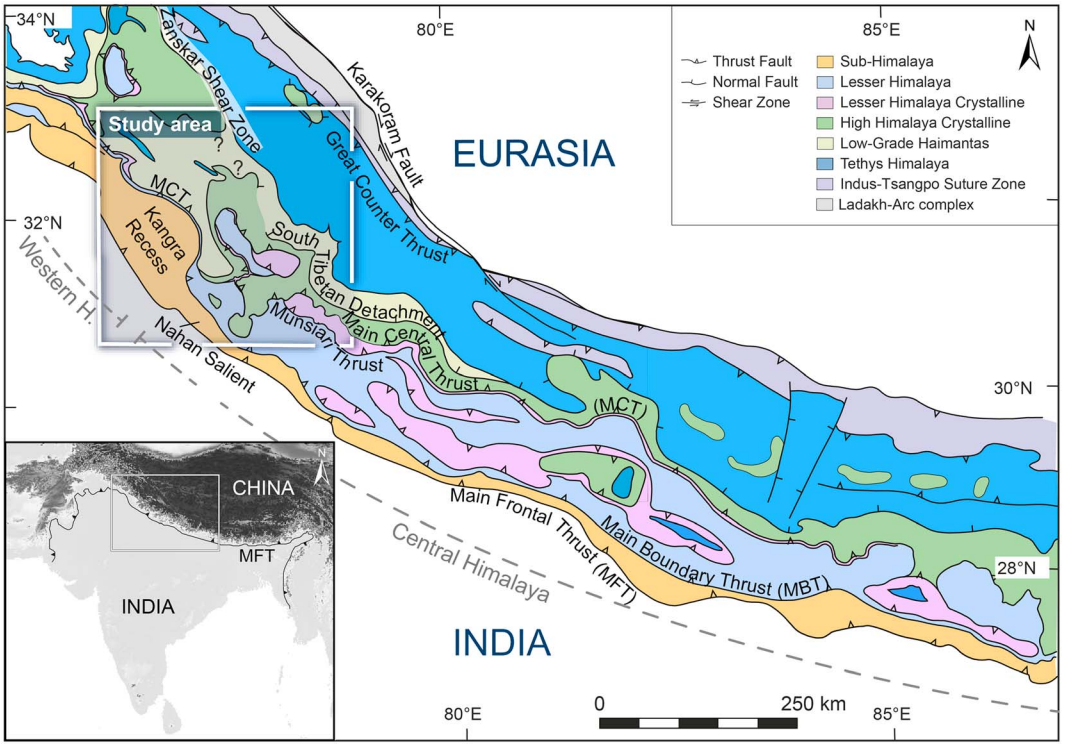

Figure 1. Geologic overview of the Himalaya between Pakistan and central Nepal. Subdivision into the Central (~91–78°E) and Western Himalaya (78–75°E) follows Hodges (2000). The rectangle shows map extent of Figure 2. Map modified after DiPietro and Pogue (2004).

In central Nepal, the southern exposures of rocks that constitute the High Himalaya are separated from the Lesser Himalaya by a pronounced change in topography known as the "physiographic transition two" (PT_2; Figure 2c; Hodges et al., 2001, Wobus et al., 2006). In most areas, the PT_2 spatially coincides with small to moderate-magnitude seismicity, and it is therefore thought to be associated with a structural and rheological change in the orogenic wedge that appears to correlate with a ramp in the Main Himalayan Thrust fault (MHT) at midcrustal level (Figure 2; Elliott et al., 2016; Mahesh et al., 2013; Pandey et al., 1995). In close proximity to the PT_2, at a distance of ~100–150 km north of the MFT, an ~30- to 40-km-wide, relatively continuous belt of rapid exhumation extends from central Nepal in the east to the Sutlej area in the west (Figure 2; e.g., Herman et al., 2010; Thiede et al., 2009; van der Beek et al., 2016). Rapid exhumation on the order of 2–5 mm/year (Jain et al., 2000; Thiede & Ehlers, 2013, and references therein) in this area has been related to the growth of a duplex structure in Lesser Himalayan rocks (e.g., Bollinger et al., 2004; Cattin & Avouac, 2000; DeCelles et al., 2001; Herman et al., 2010; Robinson et al., 2001) and/or to out-of-sequence thrusting (e.g., Whipple et al., 2016; Wobus et al., 2005). However, along-strike disparities in topography, seismicity and convergence rates suggest that orogenic growth and exhumation may not be as evenly distributed as suggested earlier. For example, there exist striking differences in topography, such as the disappearance of the PT_2 at the transition from the Central to the Western Himalaya at ~77°E (e.g., Bookhagen & Burbank, 2006; Deeken et al., 2011; Hodges, 2000; Morell et al., 2017). Coincident with this topographic transition is a change toward more limited exposure of Lesser Himalayan units and more extensive exposure of High Himalayan units and, in particular, lower-grade metamorphic High Himalayan rocks (the "low-grade Haimantas", which correspond to the light-green unit in Figure 1). To date, the underlying causes for the along-strike topographic and tectonic transition in this area has not been resolved.

In this study we document the regional exhumation patterns and their along-strike variations. We analyzed 26 new apatite fission track samples from the Beas and Chandra valleys, Himachal Pradesh, India. We combined our new data with previously published low-temperature thermochronometry and geomorphic observations to better understand the temporal and spatial evolution of first-order fault systems such as STD since the Miocene. In addition, we attempted to unravel which mechanisms ultimately account for the change in

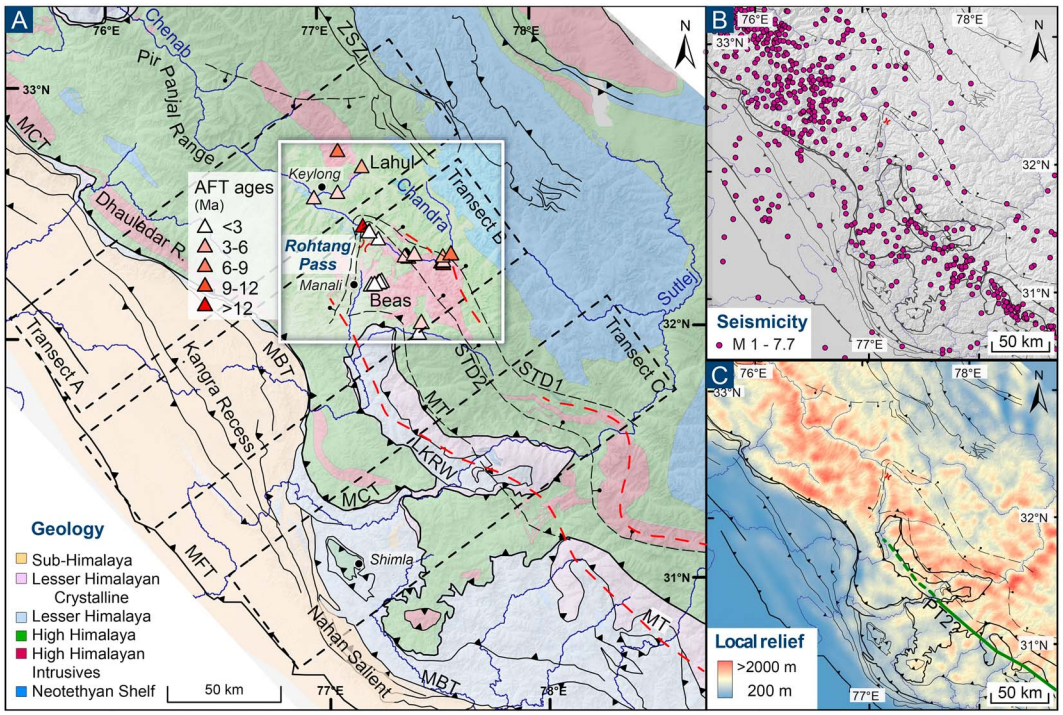

Figure 2. Geologic and physiographic overview of the study area. (a) Geological map after Steck (2003), Webb et al. (2007), Célérier et al. (2009), and Webb et al. (2011). New sample locations presented as colored triangles. The dashed rectangular boxes show the location of three transects presented in Figures 3 and 7. The dashed red lines indicate the extent of the belt of rapid exhumation as defined in text (Thiede et al., 2009). The Rohtang Pass is shown by a saddle symbol. MFT = Main Frontal Thrust, MBT = Main Boundary Thrust, MCT = Main Central Thrust, MT = Munsiari Thrust, STD = South Tibetan Detachment; ZSZ = Zanskar Shear Zone; LKRW = Larji-Kullu-Rampur window. (b) Seismicity between 1964 and 2014; events $1 < M < 5$ for locations 77°–81°E (Mahesh et al., 2013) and $4 < M < 7.7$ for other areas from the NEIC Catalog. (c) Local relief calculated from an ASTER GDEM (a product of the NASA and METI) 30-m-resolution digital elevation model, using a circular moving window with a 4.5 km radius. The green line indicates the PT_2.

exhumation style and pattern at the transition between the Western and the Central Himalaya, approximately at ~77°E. By reviewing our new and previously published data, we were able to localize the spatial characteristics of rapid exhumation and detected significant gradients in exhumation since the Miocene, both along-strike and across-strike of the orogen.

2. Topographic and Geologic Setting of the Study Area

Our study area is located in the upper part of the Beas and Chandra valleys in the state of Himachal Pradesh, India (Figures 1 and 2). The region constitutes a high-relief area, and elevations are mostly >2,000 m above sea level (asl; Figures 2c and 3). Present-day annual rainfall decreases from >2,000 mm/year south of the Rohtang Pass to less than a few hundred mm/year north of it. Moving along-strike of the orogen to the southeast and northwest from our study area, the topography and associated patterns of relief and rainfall change significantly (Figure 3). In the vicinity of the Sutlej Valley, elevation increases gradually from <1,000 m in the foreland to ~6,000 m in the orogenic interior, where deep incision of the Sutlej River has created high local relief. Rainfall is more evenly distributed across the mountain range and decreases northward more gradually. In contrast, farther northwest, in the area of the Kangra recess, elevations increase more abruptly from the Sub-Himalaya at the mountain front to >5,000 m over a very short distance, and so do rainfall and local relief.

The lower part of our study area straddles the Larji-Kullu-Rampur window (LKRW), which exposes Lesser Himalayan Crystalline and meta-sedimentary units that are separated from the low-grade to unmetamorphosed Lesser Himalayan rocks by the Munsiari or Ramgarh Thrust faults (MT or RT; e.g., Steck, 2003; Stübner et al., 2018; Webb, 2013). Rocks exposed within the LKRW define an antiform (Steck, 2003; Webb,

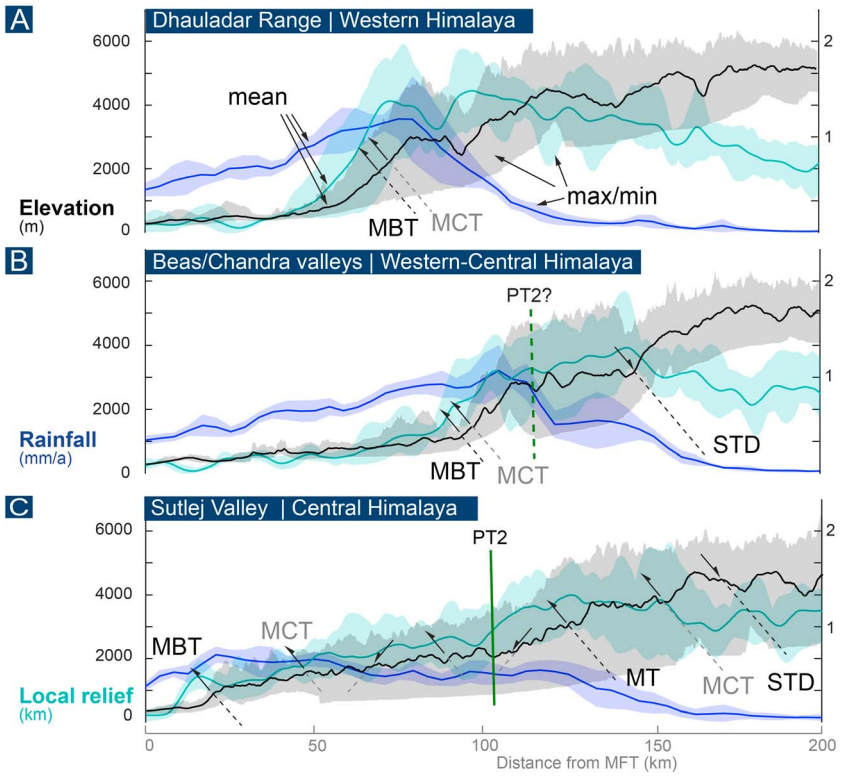

Figure 3. Swath profiles from the study area. Each panel shows elevation (black), local relief (green), and rainfall (blue) statistics (mean, min, and max), calculated over a width of 50 km. The main faults cutting the transects are indicated by dashed lines (Steck, 2003). For locations see Figure 2. PT_2 corresponds to its course in Figure 2c. Elevation data are based on ASTER GDEM (a product of NASA and METI), and rainfall is based on Tropical Rainfall Measuring Mission data (Bookhagen & Burbank, 2006).

2013) and are surrounded by the High Himalayan Crystalline complex that consists of meta-igneous and meta-sedimentary rocks (Steck, 2003). During the Miocene, the STD (top-to-the-NE) and MCT (top-to-the-SW) exhumed the high-grade core of the Himalaya, which is exposed in the High Himalayan Crystalline complex; this feature disappears toward the northwest (Vannay et al., 2004). Deformation features exposed within the High Himalayan units are mostly ductile (e.g., Steck, 2003; Webb et al., 2011). Previous work inferred that the STD, whose exact location is debated, runs through the Beas and Chandra valleys; the temporal and spatial evolution of the STD has not been understood until now (e.g., Steck, 2003; Stübner et al., 2018; Webb et al., 2007). To the south, the MCT emerges in the vicinity of the MBT around the Kangra recess.

Previous studies (e.g., Adams et al., 2009; Adlakha et al., 2013; Jain et al., 2000; Kumar et al., 1995; Lal et al., 1999; Schlup, 2003; Thiede et al., 2004, 2005, 2006, 2017; Vannay et al., 2004) have shown that the High Himalaya in the northwestern sector of the mountain belt has undergone rapid exhumation since the Late Miocene-Pliocene. Young apatite fission track (AFT) cooling ages (<3 Ma) have been reported from the Beas and Sutlej valleys and the Garhwal Himalaya (Thiede et al., 2009). North of the Kangra recess, young AFT and zircon helium (ZHe) cooling ages have been documented in the Dhauladar Range, located in the hanging wall of the MBT (Deeken et al., 2011; Thiede et al., 2017).

3. Methods

We collected samples from meta-sedimentary and meta-igneous rocks. Apatite grains were recovered from whole-rock samples using standard magnetic and heavy-liquid separation procedures. Fission track mounts were prepared and analyzed at the University of Potsdam and the University of Göttingen. After etching spontaneous tracks in 5.5 M nitric acid for 20 s at 21 °C, samples and Goodfellow mica external detectors

were irradiated at the research reactor of the Oregon State University. Mica detectors were etched in 40%-hydrofluoric acid for 45 min as described in Sobel and Strecker (2003). We determined zeta-ages (Hurford & Green, 1983). Because of the young AFT ages, several samples contain grains of zero-track densities, which partly explain why the χ^2 values of some samples are below 5%, and these samples failed the χ^2 test. For these samples, we used central ages. Samples that passed the χ^2 test with values >5% are reported as pooled ages (Galbraith, 1981; Green, 1981). All our ages listed in Table 1 were calculated with Trackkey (Dunkl, 2002).

We measured the diameter of the etch pit parallel to the *c* axis (Table 1; D_{par}) to assess the resistance of tracks to thermal annealing. D_{par} depends primarily on kinetic characteristics of the crystal (Ketcham et al., 1999) and to a lesser extent on the etching conditions (Sobel & Seward, 2010). Smaller D_{par} values (<1.75 μm) indicate low resistance to annealing; this means that annealing may occur even at lower temperatures, and relatively quickly (Donelick, 2005). We corrected for our D_{par} values following the procedure outlined in Sobel and Seward (2010).

4. Results

We analyzed a total of 26 samples: 19 from the Chandra and Chenab valleys and 7 from the Beas Valley. Sample lithologies comprise meta-sediments, gneiss, and leucogranites. Fourteen samples stem from three separate elevation transects; one elevation transect in the Beas Valley ranges from 2,383 to 4,145 m asl, two transects from the Chandra Valley range from 3,130 to 4,691 m asl. The latter include the proposed location of the STD (Webb, 2013). All samples are from the MCT hanging wall. Except for the proposed STD, no significant faults have been documented in the sampling area in the past (e.g., Epard et al., 1995; Webb et al., 2007). However, during fieldwork we were able to visit the Rohtang tunnel project where an approximately 1-km-wide cataclastic zone is exposed 3 km north of the tunnel entrance. Our new AFT cooling ages range from 1.7 ± 0.2 to 13.6 ± 1.7 Ma (Table 1 and Figure 4; errors are quoted at the 1σ level). D_{par} measurements of 1.46 ± 0.16 to 1.85 ± 0.37 μm indicate approximately homogenous track-pit sizes with little intra-sample variability. This indicates that most of our samples annealed relatively fast at low temperatures (Donelick, 2005).

Sample ages from the Beas and Parbati valleys range from 1.7 ± 0.2 to 3.4 ± 0.5 Ma with an increase in age with elevation of ~1.3 Myr/1,600 m (~1.2 mm/year; Figure 5a). In the Chandra Valley, AFT ages range from 2.3 ± 0.3 to 10.0 ± 1.1 Ma (Figure 4). The youngest cooling ages in the Chandra Valley (<3 Ma) correspond to elevations of ~3,200–3,500 m asl, immediately north of the Rohtang Pass. In two elevation transects located in the Chandra Valley, the ages increase up to ~9 Ma with a gradient of ~5 Myr/1,500 m (0.3 mm/yr; Figure 5b); these data exhibit unusually pronounced age scatter and errors, compared to many other age-elevation transects in the northwestern Himalaya (Thiede et al., 2009). Farther northwest and northeast, older (~5–10 Ma) AFT ages are also found at lower elevations (3,100–3,900 m asl; Figure 4).

Sample #9 (PE12_047; 13.6 ± 1.7 Ma) is significantly older than samples #19 and #10 (807A1 and PE12_053; 2.3 ± 0.3 and 2.5 ± 0.3 Ma) from similar elevations and at a distance of ~400 m (Figures 4 and 5b). Because younger ages are also documented farther northwest (#4 and #16; 3.7 ± 0.6 and 5.2 ± 0.7 Ma), we interpret sample #9 as an outlier, which we therefore did not include in Figure 7. Our new ages are in good agreement with previously published AFT ages from the Beas and Chandra valleys (Schlup, 2003) and help to better constrain existing regional age trends and the regional 3-D pattern of exhumation in this region.

5. Discussion

5.1. Age-Elevation Profiles and Exhumation Rates

In Figure 5, we combine our new AFT data from the Beas and Chandra valleys with ZHe ages from Stübner et al. (2018), which stem from the same sample locations. To better constrain the timing and magnitude of exhumation-rate changes in the High Himalaya, we constructed a composite vertical pseudo-elevation transect using AFT, ZHe, ZFT, and $^{40}Ar/^{39}Ar$ data (Reiners et al., 2003) from the two valleys. In this transect, AFT ages are given with their true elevations, but for ZHe, ZFT and muscovite $^{40}Ar/^{39}Ar$ data elevations increase assuming closure temperatures of 120 ± 10 and 200 ± 10, 240 ± 10, and 350 ± 50 °C for AFT, ZHe, ZFT, and muscovite $^{40}Ar/^{39}Ar$, respectively (Gleadow & Duddy, 1981; Reiners et al., 2002; Reiners & Brandon, 2006). We assume a high Pliocene geothermal gradient of 35 °C/km in agreement with previous studies (Deeken et al., 2011;

Tectonics

10.1029/2017TC004752

Table 1
Apatite Fission Track (AFT) Data From the Beas and Chandra Valleys

Nr.	Sample	Lithology	Latitude (°N)	Longitude (°E)	Altitude m	Xl[a]	Rho-S[b] (×10^6)	NS[c]	Rho-I[b] (×10^5)	NI[c]	P (χ^2)[d] (%)	Rho-D[e] (×10^6)	ND[f]	Age Ma	1σ	D_{par} (μm)	SD (μm)	Analyst[g]
1	RT11-39	Two-mica gneisss	32.2755	77.5746	4330	16	0.775	62	16.179	1295	4	8.680	3661	9.1	1.7	1.50	0.19	PE
2	RT11-28	Two-mica gneisss	32.7339	77.0902	4770	33	1.427	289	24.666	4997	2	8.610	3661	10.0	1.1	1.55	0.16	PE
3	RT11-29	Sandy siltstone of the Haimantas	32.6677	77.2016	3410	26	0.673	67	12.688	1263	16	8.530	3661	8.7	1.3	1.57	0.17	PE
4	RT11-30	Sandy siltstone of the Haimantas	32.5662	77.0865	3240	36	0.516	70	16.142	2189	19	8.460	3661	5.2	0.7	1.62	0.29	PE
5	PE12_014	Metamorphic granite	32.2834	77.5665	4599	39	1.035	316	23.766	7257	14	7.460	2962	6.3	0.6	1.74	0.30	PE
6	PE12_015	Coarse gneiss	32.2816	77.5638	4691	34	1.451	200	23.322	3215	25	7.430	2962	8.9	0.9	1.64	0.30	PE
7	PE12_017	Coarse gneiss	32.2858	77.5742	4495	35	0.957	234	24.427	5975	18	7.370	2962	5.6	0.6	1.64	0.26	PE
8	PE12_021	Medium grained granite	32.3128	77.6110	3975	21	2.221	252	37.768	4286	14	7.310	2962	8.3	0.8	1.65	0.29	PE
9	PE12_047	Medium- to coarse grained gneiss	32.4334	77.2016	3124	41	0.407	104	4.204	1073	14	7.250	2962	13.6	1.7	1.48	0.28	PE
10	PE12_053	Medium- to coarse grained gneiss	32.3807	77.2729	3214	40	0.272	73	16.259	4364	81	7.220	2962	2.3	0.3	1.76	0.25	PE
11	PE12_054	Medium- to coarse grained gneiss	32.3042	77.4110	3505	26	0.248	37	9.367	1400	100	7.190	2962	3.7	0.7	1.50	0.36	PE
12	PE12_059	Schist	32.3055	77.5734	3786	34	0.806	155	17.477	3360	6	7.160	2962	6.1	0.7	1.65	0.31	PE
13	PE12_065	Meta-sediment and gneiss	32.3113	77.4049	3130	43	0.336	108	7.757	2494	43	7.130	2962	6.0	0.7	1.68	0.32	PE
14	PE12_066	Metasediment	32.3111	77.4003	3983	32	0.269	43	7.696	1232	60	10.682	4529	7.2	1.2	1.85	0.37	PE
15	PE12_068	Metasediment	32.3105	77.3935	3570	32	0.572	64	13.333	1491	6	7.070	2962	5.9	0.9	1.46	0.23	PE
16	RT11-31	Mica-rich sandstone of the Haimantas	32.5480	76.9756	2890	39	0.473	42	17.460	1549	96	7.040	2962	3.7	0.6	1.46	0.26	PE
17	B03B4	Hbl-bearing metasediment	32.3155	77.4400	3894	80	0.464	127	17.070	4671	54	7.215	7887	3.8	0.4	-	-	KS
18	804C1	Granite	32.3132	77.6109	4053	60	2.254	465	34.219	7060	41	7.267	7887	9.3	0.5	-	-	KS
19	807A1	Augengneiss	32.4079	77.2295	3474	136	0.178	119	10.500	7006	0	7.319	7887	2.5	0.3	-	-	KS
20	823G1	Leucogranite	32.0013	77.4511	2236	180	0.103	66	8.988	5766	72	7.424	7887	1.7	0.2	-	-	KS
21	010A1	Augengneiss	32.1972	77.2350	2383	120	0.139	120	11.947	10309	43	7.581	7887	1.7	0.2	-	-	KS
22	010D1	Augengneiss	32.2045	77.2674	3356	179	0.132	84	9.121	5819	0	7.633	7887	2.2	0.3	-	-	KS
23	011B1	Granitic augengneiss	32.2120	77.2828	4145	180	0.200	128	10.137	6503	0	7.685	7887	3.0	0.3	-	-	KS
24	011D1	Granitic augengneiss	32.2070	77.2734	3484	55	0.136	53	11.054	4303	12	7.738	7887	1.9	0.3	-	-	KS
25	011E1	Leucogranite	32.1999	77.2500	2851	80	0.228	65	15.295	4361	1	7.790	7887	2.3	0.3	-	-	KS
26	014B2	Quartzite	32.0429	77.4649	3443	125	0.073	42	3.328	1907	53	7.842	7887	3.4	0.5	-	-	KS

[a]The number of individual grains dated. [b]Rho-S and rho-I are spontaneous and induced track densities measured in tracks/cm^2. [c]NS and NI are the number of spontaneous and induced tracks counted. [d]P (chi) sq (%) is the chi-square probability (Galbraith, 1981; Green, 1981). [e]Rho-D is the induced track density in external detector adjacent to CN5 dosimetry glass in tracks/cm^2. [f]ND is the number of induced tracks counted on the U standard. [g]Zeta calibration use for apatite Patricia Eugster PE 386.1 ± 27.8, Konstanze Stübner KS 389.1 ± 6.8. The D_{par} correction factor compared to Durango and Fish Canyon Tuff apatite (Donelick et al., 1999; Sobel & Seward, 2010) is 1.05 for PE.

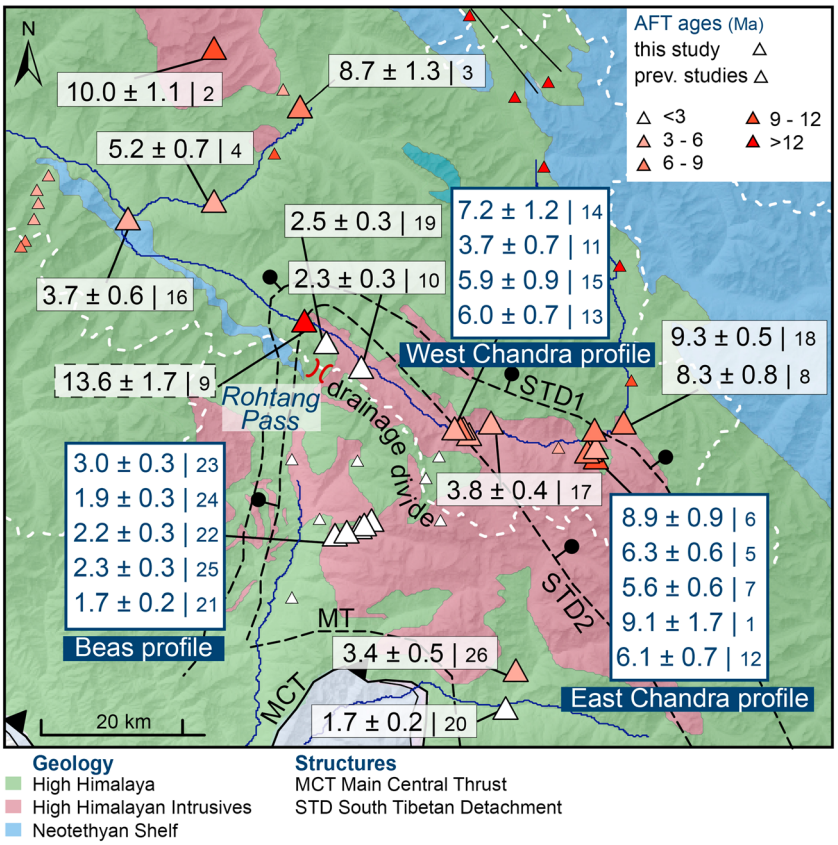

Figure 4. New and published apatite fission track data from the upper Beas and Chandra valleys. The small boxes highlight the sample age (with uncertainties) and sample number (in small fonts; cf., Table 1). The blue framed samples were collected along elevation transects shown in Figure 5. Geological map in the background is the same as in Figure 2a.

Stübner et al., 2018). Although the analyzed zircons show high U and Th (eU) compositional variation, the repeated accuracy of similar ages of our samples documents that no systematic variation is recognized, most likely related to the rapid exhumation (>1 mm/year). Ages from samples that were collected south of the Rohtang Pass (Figure 5a) display a relatively consistent trend of the combined ZHe and AFT ages (note that open symbols are from samples away from the elevation transect); the gradient of ~0.65 Myr/km suggests exhumation with near-constant rates through this temperature range since at least ~4 Ma. To facilitate regional comparison of exhumation rates, we estimate a first-order exhumation rate using the simple 1-D-modeling AGE2EDOT approach (Brandon et al., 1998) and using the same parameters as in studies from adjacent areas (i.e., model thickness, 10–30 km; geothermal gradient, 35 °C/km; Deeken et al., 2011; Thiede et al., 2009). Mean AFT ages of ~2–3 Ma in the Beas-Parbati region imply erosion rates of ~1–2 mm/year, similar to erosion rates of ~1–2 mm/year obtained from mean ZHe ages of ~3–5 Ma. The AGE2EDOT model is based on the assumption that erosion rates have been constant long enough that the thermal field achieved a dynamic equilibrium. We evaluate this assumption using RESPTIME, which calculates the advection velocity of closure isotherms, normalized to the assumed erosion rate, as a function of time since the onset of erosion (Brandon et al., 1998). Using the same parameters as for AGE2EDOT, we find that after 4 Myr of erosion, the closure-temperature isotherms of AFT and ZHe advect at 10% and 20% of the imposed erosion rate, respectively, suggesting near-steady state thermal conditions (Reiners & Brandon, 2006). Even though, in near-steady state, the closure-temperature isotherms were presumably not subhorizontal at the onset of erosion due to previous advection. Therefore, we propose that the High Himalaya south of the Rohtang Pass has been exhuming at ~1–2 mm/year since at least 4 Ma. The available data south of the Rohtang Pass do not provide any additional information, as to when this rapid exhumation began. However, the data from the north (see discussion below) and thermal modeling results of Stübner et al. (2018) suggest that the present-day pattern has been established since

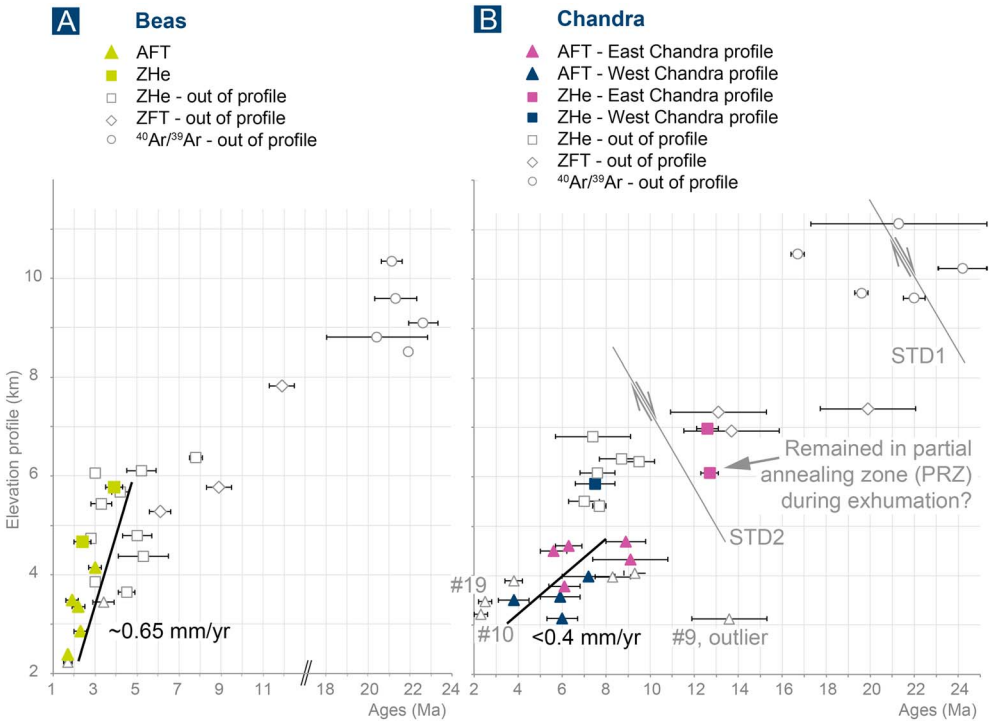

Figure 5. New AFT and published ZHe (Stübner et al., 2018), ZFT (Schlup, 2003), and $^{40}Ar/^{39}Ar$ (Schlup, 2003; Stübner et al., 2014) cooling ages, plotted against their pseudo-elevation from (a) the Beas Valley and (b) the Chandra Valley; see Figure 4 for location. Figure 5b includes the suggested $STD_{(1)}$ and $STD_{(2)}$. The grey open symbols correspond to off-profile samples. See text for definition.

8–10 Ma. The overall cooling pattern across the Rohtang Pass is most likely controlled by oblique upward thrusting along several active out-of-sequence basement thrust, in the Beas region most likely related to faulting along the MT (Stübner et al., 2018).

AFT ages from the Chandra Valley, and corresponding ZHe ages (Stübner et al., 2018), are generally older than those from south of the pass, and especially, the AFT chronometer shows significant variability in the ages of samples from similar elevation. Within the Chandra Valley we observed two cooling stages: (a) rapid cooling between 13 and 7 Ma based on ZHe, ZFT cooling ages (Figure 6) and (b) slow cooling between 9 and 3 Ma based on the age patterns of the AFT data (~0.3 mm/year). During that time the large scatter of ages from the AFT samples indicate that they must have stayed within or moved slowing through the partial annealing zone. AFT ages $<$3 Ma near to, but north of the Rohtang Pass, indicate rapid cooling during the last 3 Ma (~1 mm/year). ZHe both to the north and west of Rohtang are $>$12 Ma and indicate slow exhumation rates of $<$0.5 mm/year since the middle Miocene. One possible explanation for this cooling scenario is the movement of the rocks north of the Rohtang Pass over a ramp-flat-ramp structure, where rapid cooling occurs when the rocks pass over the ramps, while slow cooling occurs when the rocks move along the flat.

Whatever the true exhumation path is, the data show a strong increase of age with (pseudo-)elevation (~10 Myr/4,000 m; 0.4 mm/year; Figure 5b), suggesting slower late Miocene to Pliocene erosion and exhumation compared to the Beas Valley. We use the slope of the age-elevation trend (~0.3 mm/year) as an apparent exhumation rate in the Chandra Valley, because of the steep spatial gradients in AFT and ZHe ages in the upper Chandra Valley toward middle Miocene AFT ages over a distance of only a few kilometers (Schlup, 2003; this study; Figure 4). For example, the $>$10 AFT,~12–20 Ma ZHe, and $>$15 ZFT cooling ages could reflect partially reset and nonreset ages since the middle Miocene and reflect a mean exhumation $<$0.3 mm/year since that time. These cooling ages stem from the hanging wall of Zanskar shear zone and $STD_{(1)}$ and document no tectonic exhumation (fault activity) since the middle Miocene along the $STD_{(1)}$ or Zanskar Shear Zone (Figures 5b and 6). We note that the present-day orographic barrier coincides with a pronounced northward increase of AFT and ZHe cooling ages from Pliocene to middle Miocene in the upper Chandra Valley and

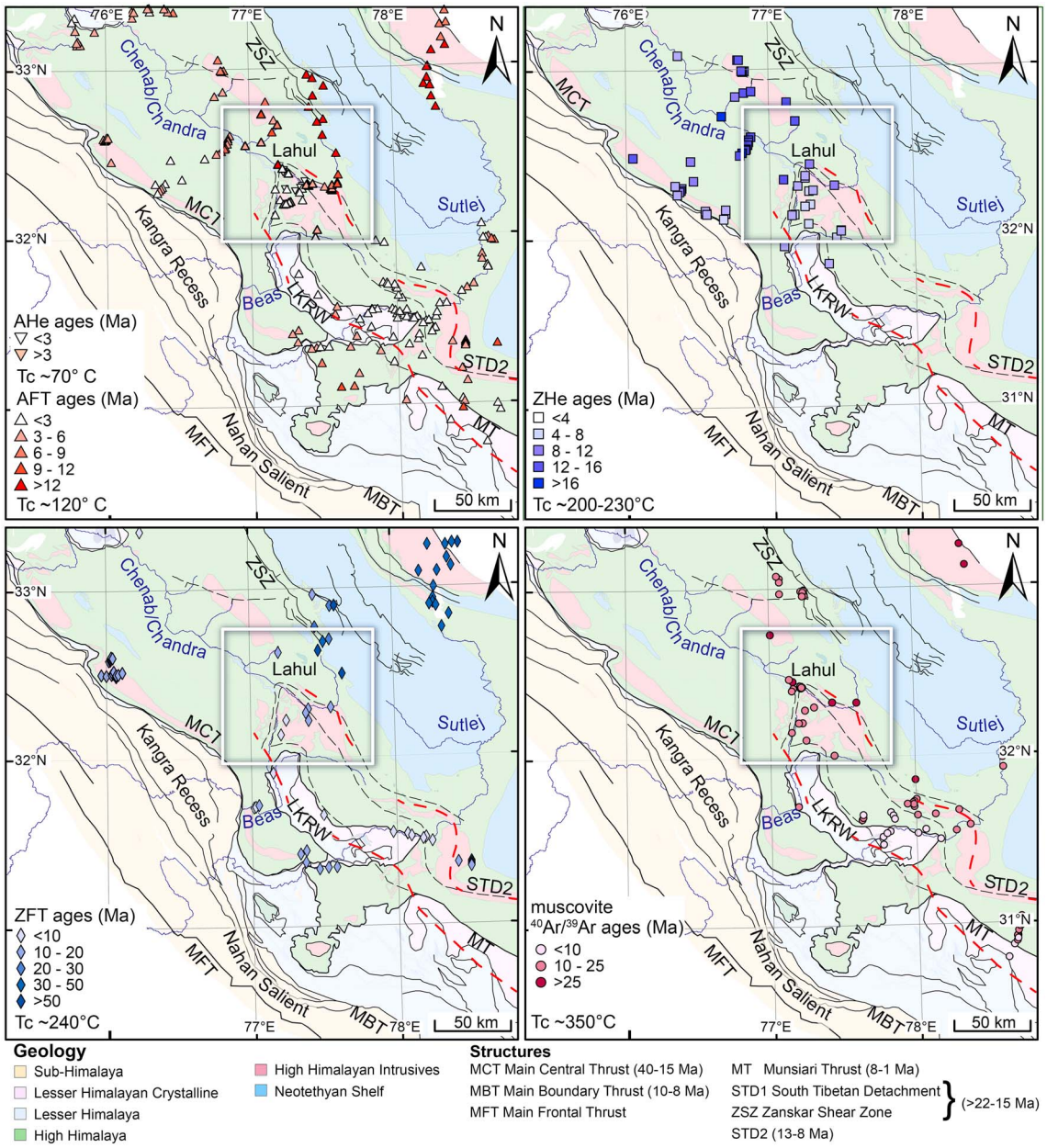

Figure 6. Overview of published and new thermochronometry data from the study area (rectangle) and adjacent regions. Data sources: Kumar et al. (1995), Dèzes et al. (1999), Lal et al. (1999), Jain et al. (2000), Schlup (2003); Thiede et al. (2004), Vannay et al. (2004), Thiede et al. (2005), Thiede et al. (2006), Adams et al. (2009), Adlakha et al. (2013); Stübner et al. (2014); Stübner et al. (2017); Thiede et al. (2017); Stübner et al. (2018). Closure temperatures (Tc) after Wolf et al. (1998), and Farley (2000) for apatite U/Th-He (AHe), Gleadow and Duddy (1981) for apatite fission track (AFT), Reiners et al. (2002) for zircon U/Th-He (ZHe), Brandon et al. (1998) for zircon fission track (ZFT), and Hodges (1991) for muscovite $^{40}Ar/^{39}Ar$. LKRW = Larji-Kullu-Rampur window. The red dashed lines indicate extent of the belt of rapid exhumation and see text for definition.

beyond. A possible conclusion is that the location of the topographic crest of the High Himalaya may have already existed here by the middle Miocene and that the orogenic interior (Lahul) may thus have been characterized by more arid conditions since then. However, we also note that during this time, the locus of active deformation and rock uplift was different from the present, and thus, the position of the high topography and the orographic barrier may have been quite different.

In contrast, samples and cooling patterns south of the Rohtang Pass exhibit continuous rapid denudation (AFT 1–3 Ma, ZHe 2–5 Ma, and ZFT 6–9 Ma) since at least late Miocene time (Schlup et al., 2011; Stübner et al., 2018). In contrast to the Chandra Valley, the cooling pattern suggests that rocks are moving continuously

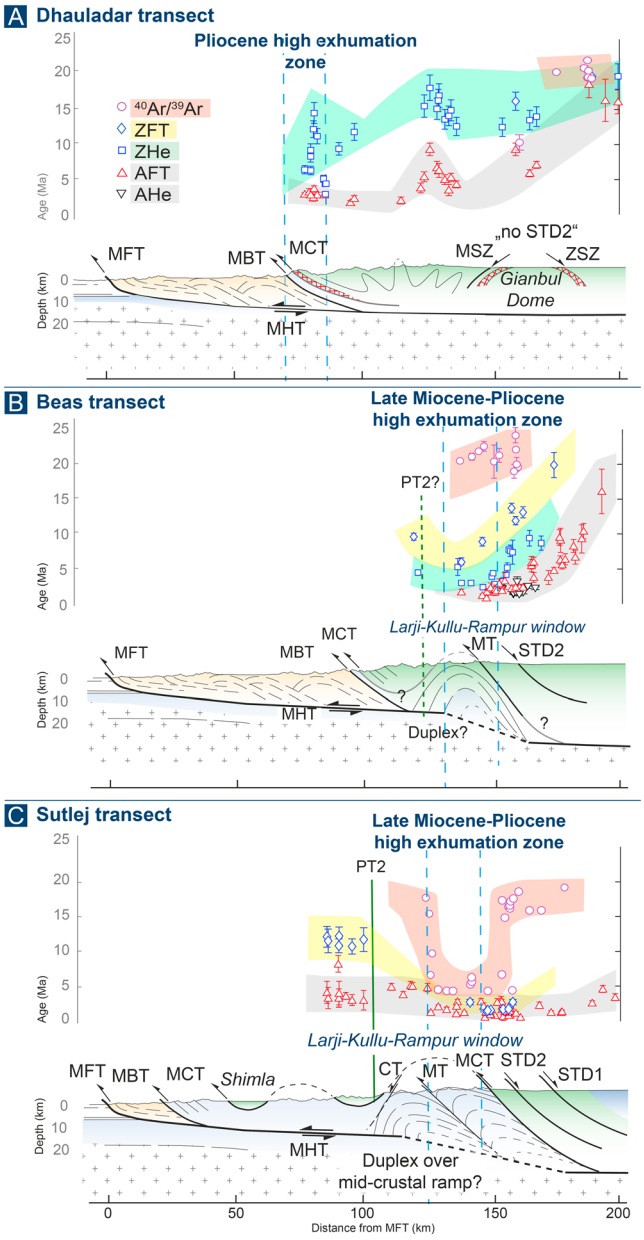

Figure 7. Transverse profiles across (a) the Dhauladar range, (b) the Beas and Chandra valleys, and (c) the Sutlej Valley. In each transect, the upper panel shows the respective thermochronometer cooling ages (Adams et al., 2009; Dèzes et al., 1999; Jain et al., 2000; Kumar et al., 1995; Lal et al., 1999; Schlup, 2003; Stübner et al., 2014, 2017; Stübner et al., 2018; Thiede et al., 2004, 2005, 2006; Thiede et al., 2017; Vannay et al., 2004). The lower panel shows inferred subsurface geometry; beneath the Dhauladar Range a steeply dipping frontal ramp is proposed to cause rapid exhumation at the MBT (Thiede et al., 2017), where no evidence for $STD_{(2)}$ activity exists. In the Beas/Chandra valleys and the Sutlej Valley, combined deformation related to the growth of the Lesser Himalayan duplex occurs; here, rocks move over a midcrustal ramp, and active faulting in the hanging wall leads to high local relief and rapid exhumation. Please note that the physiographic transition 2 (PT_2) is well defined in the Sutlej transect but disappears farther northwest (see Figure 2c).

over deep-seated ramps from depths >6 km (assuming a thermal gradient 35°/km), most likely related to the MT (Stübner et al., 2018; Vannay et al., 2004). This zone of rapid cooling along the Beas is exposed along a 20- to 30-km-long, NE-SW oriented transect; this indicates that the area is too wide to be a single exhuming block, which is moving over a ramp. This therefore suggests the existence of several ramps and/or basement thrust ramps.

In summary, the regional cooling pattern illustrates that the exhumation pattern of the study area is episodic. During the late Oligocene to early Miocene, thrusting along the MCT and extrusion along the $STD_{(1)}$ exhumed the GHS rapidly from ~20- to 30-km depth to shallow crustal depth resulting in cooling below the muscovite $^{40}Ar/^{39}Ar$ closure temperature by ~21 to 15 Ma (Schlup et al., 2011; Stübner et al., 2014; Vannay et al., 2004). Results of previous thermal modeling studies (Stübner et al., 2018; Thiede et al., 2009) suggest that low (~0.3 mm/year) middle Miocene exhumation rates in central Himachal Himalaya can be attributed to a shallow dip of the MCT (Stübner et al., 2018). This reveals two temporal and spatially varying stages of rock exhumation in the footwall of the STD, which we separated into an early phase (late Oligocene to early Miocene) referred to as $STD_{(1)}$ and a second late phase (middle to late Miocene) as $STD_{(2)}$. This second phase is constrained by ZFT and ZHe-data between 13 and 7 (Figure 6). In the Beas region the location of the STD is stable; in the Sutlej region the $STD_{(2)}$ is moving into the footwall (Figure 2). During the late Miocene-Pliocene exhumation due to accretion processes and stacking of crustal nappes along the MHT have lead to the development of the Lesser Himalayan duplex and the LKRW antiform to the south. During this time a major fault ramp has been established in the hanging wall of the Lesser Himalayan duplex (Stübner et al., 2018; Vannay et al., 2004). Rapid exhumation above this ramp is reflected by an ~40-km-wide belt of Pliocene ZFT, ZHe, and AFT cooling ages northeast of the LKRW (Schlup et al., 2011; Stübner et al., 2018; Thiede et al., 2009, and this study). These results agree with earlier interpretations that the periodicity of exhumation is caused by the passage of material points over ramp and flat segments of the basal detachment as well as out-of-sequence fault zone in the hanging wall resulting in variable rock uplift rates in space and time (Stübner et al., 2018).

Using the similar AGE2EDOT approach, Deeken et al. (2011) obtained exhumation rates of ~1 mm/year in the Dhauladar Range (cf., Figures 2 and 3) and ~0.5 mm/year in the Pir Panjal Range during the middle Miocene to Pliocene. This northward decrease in erosion rates is similar to the patterns obtained for the Beas Valley. Thiede et al. (2009) and Stübner et al. (2018) obtained exhumation rates of 2–3 mm/year since the late Miocene-Pliocene in the Sutlej and Beas valleys, respectively. The higher erosion rates suggested by Stübner et al. (2018), compared to our estimates for the same area (2–3 mm/year versus ~1 mm/year) may result from the different modeling approaches (Pecube versus AGE2EDOT) and/or the different input data (ZHe versus AFT).

5.2. Orogen-Perpendicular Transects

For a better understanding of the observed lateral variation in exhumation patterns in light of regional-scale deformation, we integrated our results with a compilation of previously published low-temperature thermochronometry data across northwestern India (Figure 6). We illustrate the lateral

change in deformation along the transition zone between the Central and Western Himalaya using three approximately orogen-perpendicular transects, each 200 km in length and compile existing thermochronology data from a 50-km-wide swath (Figure 7, footprint of swath profiles shown in Figure 2a, and topography and rainfall along swath profile shown in Figure 3). Although the transects are located only several tens of kilometers apart from each other, the topography, fault geometry, and exhumation patterns change significantly along strike in this part of the orogen. From west to east, the three transects are situated along the Dhauladar Range (Figure 7a), which resembles a typical Western Himalaya tectonic setting; the Beas Valley (Figure 7b), marking the transition zone; and the Sutlej Valley (Figure 7c), which resembles a typical Central Himalaya tectonic setting. The structural profiles are based on earlier work in the Dhauladar Range, Lahul/Beas, and Sutlej areas (Deeken et al., 2011; Steck, 2003; Stübner et al., 2018; Thiede et al., 2017; Vannay et al., 2004; Webb, 2013). Note that we projected the thermochronology data from within each swath into the profiles, whereas structural boundaries are from the centerline. Where faults and geologic boundaries traverse the swaths obliquely, slight mismatches between structures and thermochronology data may occur.

In the Dhauladar Range (Figure 7a), young ZHe ages (<5 Ma), which constrain rapid Pliocene exhumation with rates of 2–3 mm/year, are limited to a 40-km-wide zone, immediately north of the MBT (Deeken et al., 2011; Thiede et al., 2017). Most of the MCT hanging wall is characterized by older ZHe (10–18 Ma) and AFT (~3–10 Ma) ages, reflecting mean erosion rates of ~0.5 mm/year since ~15 Ma (Deeken et al., 2011; Thiede et al., 2017). In this transect, the PT_2 is neither defined as a major physiographic transition, nor is there a swath of young cooling ages or the existence of the $STD_{(2)}$ that would correspond to rapid exhumation in the orogenic interior as identified in the Beas and Sutlej transects (Figure 7).

Along the Beas transect (Figure 7b), which includes our study area, an ~65-km-wide zone of high local relief corresponds approximately with the region northeast of the PT_2, which is less well defined here than farther to the southeast (i.e., Sutlej transect; Figures 3c and 7c). The northeastern part of this zone coincides with an ~35-km-wide band of young AFT (<3 Ma) and ZHe (<5 Ma) ages (this study; Schlup, 2003; Stübner et al., 2018). Muscovite $^{40}Ar/^{39}Ar$ ages in this sector are significantly older (~20 Ma) and have been attributed to Early Miocene extrusion between MCT and $STD_{(1)}$ (Stübner et al., 2014), suggesting that high exhumation rates were established within this topographic band in the late Miocene (Stübner et al., 2018). Possible explanations for this rapid exhumation include thrusting over a midcrustal ramp (cf., Herman et al., 2010, and references therein), in combination with the growth of a Lesser Himalayan duplex, and/or thrusting (basement thrust ramp) along the MT (Stübner et al., 2018). Although we argue above that an orographic effect accounts for the northward decrease in erosion rates and hence an increase in cooling ages, higher rainfall is probably not the only reason for rapid exhumation, because (1) the highest mean annual rainfall occurs ~50 km southwest of the band of young cooling ages, (2) the band of young cooling ages coincides with the proposed location of an MHT ramp (Stübner et al., 2018) and the Lesser Himalayan duplex associated with the LKRW-antiform (Vannay & Grasemann, 2001; Webb, 2013), and (3) a climate-driven mechanism does not readily explain the lateral changes in exhumation pattern from the Sutlej to the Dhauladar transects (Figure 6).

Along the Sutlej transect (Figure 7c) a zone of rapid late Miocene-Pliocene exhumation is reflected by an ~25- to 60-km-wide band of young AFT and ZFT (≤5 Ma) and muscovite $^{40}Ar/^{39}Ar$ cooling ages (<8 Ma) between the MT and $STD_{(2)}$ (Jain et al., 2000; Thiede et al., 2004, 2005, 2009; Vannay et al., 2004). Extrusion of Lesser Himalayan Crystalline rocks, accommodated by thrusting on the MT since the late Miocene (Caddick et al., 2007) and possibly assisted by normal-fault reactivation of the $STD_{(2)}$ in the MCT hanging wall, accounts for young cooling ages in the MCT footwall (Vannay et al., 2004). However, Thiede et al. (2005, 2009) show that young cooling ages occur in a localized zone along the Sutlej River, which includes both MCT and $STD_{(2)}$ hanging walls and footwalls, and attribute cooling through the AFT closure temperature to protracted incision of the Sutlej River (cf., Vannay et al., 2004). Toward the southeast and northwest, the band of young AFT cooling ages is structurally bounded by the MT and $STD_{(2)}$, respectively; this suggests that the belt of young cooling ages in the Sutlej transect is related to the combined effect of tectonically driven exhumation over a midcrustal ramp and/or duplex and sustained vigorous river incision (Thiede et al., 2005; Vannay et al., 2004).

From Garhwal to central Nepal (77°E–91°E), the PT_2 consistently delineates the boundary between a moderate-relief landscape and the slowly eroding (<1 mm/year) Lesser Himalaya and a high-relief, rapidly

eroding (>1 mm/year) High Himalaya (Godard et al., 2014; Hodges et al., 2001; Morell et al., 2017; Scherler et al., 2014). The lateral changes in physiographic characteristics and exhumation rates between the Sutlej, Beas, and Dhauladar transects since ~5–10 Ma document the lateral termination of the PT_2 in the northwestern Himalaya (Figure 2c). In the Sutlej and Beas transects, the high exhumation zone north of the PT_2 corresponds to tectonically driven rock uplift above an MHT ramp or duplex (Figure 7; Stübner et al., 2018). Singh et al. (2018) document earthquake moment-tensor solutions for a seismicity cluster at depths between 5 and 10 km within the LKRW of the Sutlej transect, which are consistent with ~30° NE dipping fault planes in the Lesser Himalayan duplex. In contrast, the lower exhumation rates and older cooling ages throughout the Dhauladar transect have been attributed to a gently dipping MHT with no evidence for a ramp or a Lesser Himalayan duplex structures (Deeken et al., 2011; Thiede et al., 2017).

5.3. Potential Causes for Changes in Tectonic Style in the NW Himalaya

Various factors have been proposed to influence the tectonic style, pattern of deformation, and topography in the Himalaya in general. Amongst these are the following:

1. The far-field, plate-tectonic effects on the kinematics and the arcuate shape of the Himalaya result in westward-increasing obliquity in the convergence between India and Tibet, which ought to be associated with increasing partitioning of deformation (e.g., Kundu et al., 2014; Styron et al., 2011; Thakur et al., 2014; Whipp et al., 2014).
2. Because the amount of rainfall varies along strike of the mountain belt (e.g., Bookhagen & Burbank, 2006) from east to west, it may be assumed that erosion decreases westward and impacts the tectonic stress field, which may ultimately lead to different patterns of deformation (e.g., Willett, 1999).
3. Along-strike variations in the thickness of the Proterozoic sedimentary cover on the Indian margin may lead to variations in the style and pattern of sediment accretion and duplex formation (e.g., Raiverman et al., 1983; Rajendra Prasad et al., 2011).
4. Approximately northeast trending ridges in the Indian basement form asperities that may affect deformation and exhumation patterns in the overthrusting orogenic wedge (Arora et al., 2012). A related mechanism is the reactivation of preorogenic normal faults in the Indian basement, which may lead to the formation of lateral or oblique ramps in the basal thrust of the orogen (Dubey et al., 2004; Powers et al., 1998).

The above considerations may explain many salient features of Himalayan topography, structures, and exhumation patterns. However, a simple explanation for lateral variations, based on the presented data, is not yet possible. While some of the above factors are more likely to account for gradual and progressive along-strike changes (models 1 and 2), others are more likely to account for abrupt spatial variability (models 3 and 4). Because recent studies have suggested that tectonics—not climate—is the dominant control of the spatial pattern of erosion (e. g., Godard et al., 2014; Olen et al., 2015; Scherler et al., 2014), we focus on the scenarios (1), (3), and (4), which we consider to explain best the observed abrupt changes in geology, topography, and exhumation pattern from the Central to the Western Himalaya. In the following sections we discuss viable causes and mechanisms that may be responsible for lateral variations in tectonic style and exhumation patterns, considering the observed regional changes at the transition between the Central and the Western Himalaya.

The western termination of the PT_2 coincides with the prominent Kangra recess and a significant westward narrowing of the exposure of Lesser Himalayan rocks and a widening of the Sub-Himalaya at 77°E (Figure 1). Recesses and salients in mountain belts are commonly attributed to spatial variations in the thickness of sedimentary cover rocks that can be easily scraped off and incorporated into orogenic wedges (e.g., Macedo & Marshak, 1999). The Proterozoic Vindhyan Supergroup covers large parts of the Indian basement and underlies much of the Indo-Gangetic foreland basin (e.g., Raiverman, 2002; Valdiya, 1995; Yin, 2006). Based on seismic reflection data, Rajendra Prasad et al. (2011) demonstrate a northwestward decrease in the thickness of the Vindhyan formations and, in particular, a significant reduction in stratigraphic thickness from the Nahan salient (Sutlej transect) to the Kangra recess (Beas transect). These authors proposed that lateral variations in stratigraphic thickness and regional extent account for the salient-recess geometry at ~77°E, which affects the mechanics within the Himalayan orogenic wedge (Macedo & Marshak, 1999). These authors furthermore argue against a lateral basement ramp between the Kangra recess and the Nahan salient, for which they find no evidence in seismic reflection data (cf., Powers et al., 1998). Extending the argument of Rajendra Prasad

et al. (2011) to regional scale, one could explain the change in tectonic style from the Central to the Western Himalaya, and the lateral termination of the PT_2 in northwestern Himalaya, if the Proterozoic units were generally thicker in the east compared to the west. Such a decrease of stratigraphic thickness of the Indian sedimentary cover could account for not only the reduced width of the LHS exposure west of 77°E but also the shallower exhumation (i.e., the low-grade metamorphic Haimantas units west of Beas versus the high-grade metamorphic core to the east) and lower exhumation rates in the northwestern Himalaya.

The influx of material into orogenic wedges is, however, controlled not only by the sediment thickness but also by the convergence rate (e.g., Dahlen, 1990). It has been noted previously that the westward increase in the obliquity of the convergence direction between India and Tibet ought to be associated with increasing partitioning of deformation (e.g., Kundu et al., 2014; Styron et al., 2011; Thakur et al., 2014; Whipp et al., 2014). The Global Positioning System (GPS)-derived convergence rate between Tibet and India decreases from ~20.2 ± 1.1 mm/year in central Nepal (~83°E) to ~18.5 ± 1.8 mm/year in the northwestern Himalaya (~79°E) and ~13.3 ± 1.7 mm/year in Kashmir (~76°E; Stevens & Avouac, 2015). Kundu et al. (2014) determined ~13.6 mm/year frontal convergence in the northwestern Himalaya (~76–78°E), which is oblique to the overall orientation of the Himalayan arc. Split into an arc-normal component of 11.8 mm/year and an arc-parallel dextral component of 6.7 mm/year, this estimate may imply an even stronger westward decrease in arc-normal convergence rates. A westward decrease in arc-normal convergence will have a similar effect as a westward decrease in the thickness of the sedimentary cover: the reduced material flux into the orogenic wedge may lead to reduced exhumation within the wedge to maintain the material-flux balance (e.g., Macedo & Marshak, 1999). Sustained lower convergence rates would be associated with a westward decrease of the total amount of shortening. Although currently available data do not readily support the interpretation of a decrease of total shortening with increasing obliquity of the convergence direction (e.g., Bhattacharyya & Ahmed, 2016; DeCelles et al., 2002), we note that these estimates are notoriously difficult to obtain and fraught with uncertainties.

Finally, kinematic models of the evolution of the Himalayan orogenic wedge highlight two distinct phases; first, with long-distance overthrusting of the Tethyan Himalaya, followed by basal accretion and duplex formation leading to substantial amounts of shortening and crustal thickening (e.g., Robinson et al., 2001). The activation of duplex structures may in fact be related to the thermal and rheological evolution of the orogen and the depth of the brittle-ductile transition (e.g., Avouac, 2007). Within this context, the amount of crustal thickening and heating, which can be related to both total shortening and the thickness of cover rocks that are scraped off the lower plate, may reach a critical threshold at which duplex formation initiates. If this were true, the transition in tectonic style may be expected to migrate westward through time, and the formation of duplex structures were yet to follow in the western Himalaya.

In summary, the combination of both effects—the westward decreasing convergence rate and, consequently, total shortening, as well as potential thinning of the Proterozoic cover units—may account for the low exhumation documented in the northwestern Himalaya. However, neither of these effects predicts the relatively sharp transition from high exhumation and a well-defined PT_2 to the low exhumation as we have documented in the area between the Sutlej and Dhauladar transects. Future studies may reveal whether this sharp transition may be attributed, for example, to preexisting structures or to some threshold mechanism that controls orogenic-wedge evolution.

6. Conclusions

We presented new AFT ages and field observations from northwestern India that constrain the spatial extent and structural characteristics of the western termination of the high-exhumation belt along strike of the Himalayan arc. Our newly obtained AFT data help to better delimit the spatial extent of those parts of the Himalaya that are characterized by young cooling ages and rapid exhumation (~1–2 mm/year) of metamorphic core area of the Himalaya. This region is bounded to north and south by areas characterized by significantly older cooling ages, and therefore lower exhumation rates (≤0.4 mm/year). Our results suggest that the termination of the high-exhumation belt coincides with a northward plunging crustal-scale antiform and major out-of-sequence basement thrust along the northwestern border of the LKRW. We interpret this crustal-scale antiform to be part of the Lesser Himalayan duplex structure. We discuss possible factors that help explain the transition in tectonic style from the Central to the Western Himalaya. We hypothesize that

the combination of westward decreasing thickness in Indian cover sediments that are potentially available for underthrusting in the orogenic wedge and westwardly decreasing arc-normal shortening, due to increasingly oblique convergence and strain partitioning, may be responsible for the inferred disappearance of a midcrustal ramp, out-of-sequence basement thrust, and the formation of Lesser Himalayan duplexes.

Acknowledgments
This study was funded by DFG (Deutsche Forschungsgemeinschaft) grants to M. Strecker (STR 373/19-2; part of the graduate school GRK 1364) and R. Thiede (TH 1371/5-1) and DAAD-DST (PPP-India # 57035520) to R. Thiede and V. Jain. K. Stübner was funded by DFG grant STU 525/1-1 and the Excellence Initiative of the University of Tübingen. We thank V. Jain and T. Tsering Longpo for logistical support during the field seasons in India; P. Ballato, S. Dey, and S. Olen for helpful discussions; and J. Faruhn for assistance with sample preparation. We also thank two anonymous reviewers and the AE S. Long for their comments that increased the quality of the manuscript significantly. Data on apatite fission track cooling age calculation and rate calculations are provided in the supporting information of this manuscript.

References

Adams, B., Dietsch, C., Owen, L. A., Caffee, M. W., Spotila, J., & Haneberg, W. C. (2009). Exhumation and incision history of the Lahul Himalaya, northern India, based on (U-Th)/He thermochronometry and terrestrial cosmogenic nuclide methods. *Geomorphology*, *107*(3–4), 285–299. https://doi.org/10.1016/j.geomorph.2008.12.017

Adlakha, V., Patel, R. C., Lal, N., Mehta, Y. P., Jain, A. K., & Kumar, A. (2013). Tectonics and climate interplay: Exhumation patterns of the Dhauladar Range, Northwest Himalaya. *Current Science*, *104*(11), 1551–1559.

Arora, B. R., Gahalaut, V. K., & Kumar, N. (2012). Structural control on along-strike variation in the seismicity of the northwest Himalaya. *Journal of Asian Earth Sciences*, *57*, 15–24. https://doi.org/10.1016/j.jseaes.2012.06.001

Avouac, J. P. (2003). Mountain building, erosion, and the seismic cycle in the Nepal Himalaya. *Advances in Geophysics*, *46*, 1–80. https://doi.org/10.1016/S0065-2687(03)46001-9

Avouac, J. P. (2007). Dynamic processes in extensional and compressional settings - mountain building: From earthquakes to geological deformation. *Treatise on Geophysics*, *6*, 377–439.

Bendick, R., & Bilham, R. (2001). How perfect is the Himalayan arc? *Geology*, *29*(9), 791. https://doi.org/10.1130/0091-7613(2001)029<0791:HPITHA>2.0.CO;2

Bhattacharyya, K., & Ahmed, F. (2016). Role of initial basin width in partitioning total shortening in the Lesser Himalayan fold-thrust belt: Insights from regional balanced cross-sections. *Journal of Asian Earth Sciences*, *116*, 122–131. https://doi.org/10.1016/j.jseaes.2015.11.012

Bollinger, L., Henry, P., & Avouac, J. P. (2004). Thermal structure and exhumation history of the Lesser Himalaya in central Nepal. *Tectonics*, *23*, TC5015. https://doi.org/10.1029/2003TC001564

Bookhagen, B., & Burbank, D. W. (2006). Topography, relief, and TRMM-derived rainfall variations along the Himalaya. *Geophysical Research Letters*, *33*, L08405. https://doi.org/10.1029/2006GL026037

Brandon, M. T., Roden-Tice, M. K., & Garver, J. I. (1998). Late Cenozoic exhumation of the Cascadia accretionary wedge in the Olympic Mountains, northwest Washington State. *Geological Society of America Bulletin*, *110*(8), 985–1009. https://doi.org/10.1130/0016-7606(1998)110<0985:LCEOTC>2.3.CO;2

Burg, J. P., Guiraud, M., Chen, G. M., & Li, G. C. (1984). Himalayan metamorphism and deformations in the North Himalayan Belt (southern Tibet, China). *Earth and Planetary Science Letters*, *69*(2), 391–400. https://doi.org/10.1016/0012-821X(84)90197-3

Caddick, M. J., Bickle, M. J., & Harris, N. (2007). Burial and exhumation history of a Lesser Himalayan schist: Recording the formation of an inverted metamorphic sequence in NW India. *Earth and Planetary Science Letters*, *264*(3–4), 375–390. https://doi.org/10.1016/j.epsl.2007.09.011

Cattin, R., & Avouac, J. P. (2000). Modeling mountain building and the seismic cycle in the Himalaya of Nepal. *Journal of Geophysical Research*, *105*, 13,389–13,407. https://doi.org/10.1029/2000JB900032

Célérier, J., Harrison, T. M., & Webb, A. G. (2009). The Kumaun and Garhwal Lesser Himalaya, India: Part 1. Structure and stratigraphy. *Geological Society of America Bulletin*, *121*(9–10), 1262–1280. https://doi.org/10.1130/B26344.1

Dahlen, F. A. (1990). Critical taper model of fold-and-thrust belts and accretionary wedges. *Annual Review of Earth and Planetary Sciences*, *18*, 55–99.

DeCelles, P. G., Carrapa, B., Gehrels, G. E., Chakraborty, T., & Ghosh, P. (2016). Along-strike continuity of structure, stratigraphy, and kinematic history in the Himalayan thrust belt: The view from northeastern India. *Tectonics*, *35*, 2995–3027. https://doi.org/10.1002/2016TC004298

DeCelles, P. G., Robinson, D. M., Quade, J., Ojha, T. P., Garzione, C. N., Copeland, P., & Upreti, B. N. (2001). Stratigraphy, structure, and tectonic evolution of the Himalayan fold-thrust belt in western Nepal. *Tectonics*, *20*(4), 487–509. https://doi.org/10.1029/2000TC001226

DeCelles, P. G., Robinson, D. M., & Zandt, G. (2002). Implications of shortening in the Himalayan fold-thrust belt for uplift of the Tibetan Plateau. *Tectonics*, *21*(6), 1061. https://doi.org/10.1029/2001TC001322

Deeken, A., Thiede, R., & Sobel, E. (2011). Exhumational variability within the Himalaya of northwest India. *Earth and Planetary Science Letters*, *305*, 103–114. https://doi.org/10.1016/j.epsl.2011.02.045

van der Beek, P., Litty, C., Baudin, M., Mercier, J., Robert, X., & Hardwick, E. (2016). Contrasting tectonically driven exhumation and incision patterns, western versus central Nepal Himalaya. *Geology*, *44*(4), 327–330. https://doi.org/10.1130/G37579.1

Dèzes, P. J., Vannay, J. C., Steck, A., Bussy, F., & Cosca, M. (1999). Synorogenic extension: Quantitative constraints on the age and displacement of the Zanskar shear zone (northwest Himalaya). *Bulletin of the Geological Society of America*, *111*(3), 364–374. https://doi.org/10.1130/0016-7606(1999)111<0364:SEQCOT>2.3.CO;2

DiPietro, J. A., & Pogue, K. R. (2004). Tectonostratigraphic subdivisions of the Himalaya: A view from the west. *Tectonics*, *23*, TC5001. https://doi.org/10.1029/2003TC001554

Donelick, R. A. (2005). Apatite fission-track analysis. *Reviews in Mineralogy and Geochemistry*, *58*(1), 49–94. https://doi.org/10.2138/rmg.2005.58.3

Donelick, R. A., Ketcham, R. A., & Carlson, W. D. (1999). Variability of apatite fission-track annealing kinetics; II, Crystallographic orientation effects. *American Mineralogist*, *84*(9), 1224–1234. https://doi.org/10.2138/am-1999-0902

Dubey, A. K., Bhakuni, S. S., & Selokar, A. D. (2004). Structural evolution of the Kangra recess, Himachal Himalaya: A model based on magnetic and petrofabric strains. *Journal of Asian Earth Sciences*, *24*(2), 245–258. https://doi.org/10.1016/j.jseaes.2003.11.002

Duncan, C., Masek, J., & Fielding, E. (2003). How steep are the Himalaya? Characteristics and implications of along-strike topographic variations. *Geology*, *31*(1), 75–78. https://doi.org/10.1130/0091-7613(2003)031<0075:HSATHC>2.0.CO;2

Dunkl, I. (2002). Trackkey: A Windows program for calculation and graphical presentation of fission track data. *Computers & Geosciences*, *28*(1), 3–12. https://doi.org/10.1016/S0098-3004(01)00024-3

Elliott, J. R., Jolivet, R., González, P. J., Avouac, J. P., Hollingsworth, J., Searle, M. P., & Stevens, V. L. (2016). Himalayan megathrust geometry and relation to topography revealed by the Gorkha earthquake. *Nature Geoscience*, *9*. https://doi.org/10.1038/NGEO2623

Epard, J. L., Vannay, J. C., & Hunziker, J. C. (1995). Tertiary Himalayan structures and metarmorphism in the Kullu Valley (Mandi-Khoksar transect in the Western Himalaya)–Shikar-Beh-nappe and crystalline nappe. *Schweizerische Mineralogische und Petrographische Mitteilungen*, *75*, 59–84. https://doi.org/10.5169/seals-57144

Farley, K. A. (2000). Helium diffusion from apatite: General behavior as illustrated by Durango fluorapatite. *Journal of Geophysical Research*, *105*, 2903–2914. https://doi.org/10.1029/1999JB900348

Galbraith, R. F. (1981). On statistical models for fission track counts. *Journal of the International Association for Mathematical Geology*, *13*(6), 471–178. https://doi.org/10.1007/BF01034498

Gansser, A. (1964). *Geology of the Himalayas* (p. 289). New York: Wiley-Interscience.

Gleadow, A. J. W., & Duddy, I. R. (1981). A natural long-term track annealing experiment for apatite. *Nuclear Tracks*, *5*(1–2), 169–174. https://doi.org/10.1016/0191-278X(81)90039-1

Godard, V., Bourlès, D. L., Spinabella, F., Burbank, D. W., Bookhagen, B., Burch Fisher, G., et al. (2014). Dominance of tectonics over climate in Himalayan denudation. *Geology*, *43*(3), 243–246. https://doi.org/10.1130/G35342.1

Green, P. F. (1981). A new look at statistics in fission-track dating. *Nuclear Tracks*, *5*(1–2), 77–86. https://doi.org/10.1016/0191-278X(81)90029-9

Harvey, J. E., Burbank, D. W., & Bookhagen, B. (2015). Along-strike changes in Himalayan thrust geometry: Topographic and tectonic discontinuities in western Nepal. *Lithosphere*, *7*(5), 511–518. https://doi.org/10.1130/L444.1

Herman, F., Copeland, P., Avouac, J.-P., Bollinger, L., Mahéo, G., Le Fort, P., et al. (2010). Exhumation, crustal deformation, and thermal structure of the Nepal Himalaya derived from the inversion of thermochronological and thermobarometric data and modeling of the topography. *Journal of Geophysical Research*, *115*, B06407. https://doi.org/10.1029/2008JB006126

Hodges, K. V. (1991). Pressure-temperature-time paths. *Annual Review of Earth and Planetary Sciences*, *19*(1), 207–236. https://doi.org/10.1146/annurev.ea.19.050191.001231

Hodges, K. V. (2000). Tectonics of the Himalaya and southern Tibet from two perspectives. *Geological Society of America Bulletin*, *112*(3), 324–350. https://doi.org/10.1130/0016-7606(2000)112<324:TOTHAS>2.0.CO;2

Hodges, K. V., Hurtado, J. M., & Whipple, K. X. (2001). Southward extrusion of Tibetan crust and its effect on Himalayan tectonics. *Tectonics*, *20*, 799–809. https://doi.org/10.1029/2001TC001281

Hurford, A. J., & Green, P. F. (1983). The zeta age calibration of fission-track dating. *Chemical Geology*, *41*, 285–317. https://doi.org/10.1016/S0009-2541(83)80026-6

Jain, A., Kumar, D., Singh, S., Kumar, A., & Lal, N. (2000). Timing, quantification and tectonic modelling of Pliocene–Quaternary movements in the NW Himalaya: evidence from fission track dating. *Earth and Planetary Science Letters*, *179*(3–4), 437–451. https://doi.org/10.1016/S0012-821X(00)00133-3

Ketcham, R. A., Donelick, R. A., & Carlson, W. D. (1999). Variability of apatite fission-track annealing kinetics: III. Extrapolation to geological time scales. *American Journal of Science*, *84*, 1235–1255. https://doi.org/10.2138/am-1999-0903

Kohn, M. J. (2014). Himalayan metamorphism and its tectonic implications. *Annual Review of Earth and Planetary Sciences*, *42*(1), 381–419. https://doi.org/10.1146/annurev-earth-060313-055005

Kumar, A., Lal, N., Jain, A. K., & Sorkhabi, R. B. (1995). Late Cenozoic-Quaternary thermo-tectonic history of Higher Himalayan Crystalline (HHC) in Kishtwar-Padar-Zanskar region, NW Himalaya: Evidence from fission track ages. *Journal Geological Society of India*, *45*, 375–391.

Kundu, B., Yadav, R. K., Bali, B. S., Chowdhury, S., & Gahalaut, V. K. (2014). Oblique convergence and slip partitioning in the NW Himalaya: Implications from GPS measurements. *Tectonics*, *33*, 2013–2014. https://doi.org/10.1002/2014TC003633

Lal, N., Mehta, Y. P., Kumar, D., Kumar, A., & Jain, A. K. (1999). Cooling and exhumation history of the Mandi granite and adjoining tectonic units, Himachal Pradesh, and estimation of closure temperature from external surface of zircon, Geodynamics of the NW Himalaya. *Gondwana Research Group Memoir*, *6*, 207–216.

Macedo, J., & Marshak, S. (1999). Controls on the geometry of fold-thrust belt salients. *Geological Society of America Bulletin*, *111*(12), 1808–1822. https://doi.org/10.1130/0016-7606(1999)111<1808:COTGOF>2.3.CO;2

Mahesh, P., Rai, S. S., Sivaram, K., Paul, A., Gupta, S., Sarma, R., & Gaur, V. K. (2013). One-dimensional reference velocity model and precise locations of earthquake hypocenters in the Kumaon–Garhwal Himalaya. *Bulletin of the Seismological Society of America*, *103*(1), 328–339. https://doi.org/10.1785/0120110328

Morell, K. D., Sandiford, M., Kohn, B., Codilean, A., Fülöp, R.-H., & Ahmad, T. (2017). Current strain accumulation in the hinterland of the northwest Himalaya constrained by landscape analyses, basin-wide denudation rates, and low temperature thermochronology. *Tectonophysics*, *721*, 70–89. https://doi.org/10.1016/j.tecto.2017.09.007

National Earthquake Information Center (NEIC) (n.d.), Catalog of Global Seismicity, http://earthquake.usgs.gov/earthquakes/search/, U.S. Geol. Surv. Earthquake Data Base, Reston, Va.

Olen, S. M., Bookhagen, B., Hoffmann, B., Sachse, D., Adhikari, D. P., & Strecker, M. R. (2015). Understanding erosion rates in the Himalayan orogen: A case study from the Arun Valley. *Journal of Geophysical Research*, *120*, 2080–2102. https://doi.org/10.1002/2014JF003410

Pandey, M. R., Tandukar, R. P., Avouac, J. P., Lavé, J., & Massot, J. P. (1995). Interseismic strain accumulation on the Himalayan crustal ramp (Nepal). *Geophysical Research Letters*, *22*, 751–754. https://doi.org/10.1029/94GL02971

Powers, P. M., Lillie, R. J., & Yeats, R. S. (1998). Structure and shortening of the Kangra and Dehra Dun reentrants, Sub-Himalaya, India. *Geological Society of America Bulletin*, *110*(8), 1010–1027. https://doi.org/10.1130/0016-7606(1998)110<1010:SASOTK>2.3.CO;2

Raiverman, V. (2002). Foreland sedimentation in Himalayan tectonic regime: a relook at the orogenic process, Bishen Singh Mahendra Pal Sing, Dehra Dun (p. 378).

Raiverman, V., Kunte, S. V., & Mukherjea, A. (1983). Basin geometry, Cenozoic sedimentation and hydrocarbon prospects in northwestern Himalaya and Indo-Gangetic plains. *Petroleum Asia Journal*, *6*, 67–92.

Rajendra Prasad, B., Klemperer, S. L., Vijaya Rao, V., Tewari, H. C., & Khare, P. (2011). Crustal structure beneath the Sub-Himalayan fold–thrust belt, Kangra recess, northwest India, from seismic reflection profiling: Implications for late Paleoproterozoic orogenesis and modern earthquake hazard. *Earth and Planetary Science Letters*, *308*(1–2), 218–228. https://doi.org/10.1016/j.epsl.2011.05.052

Reiners, P. W., & Brandon, M. T. (2006). Using thermochronology to understand orogenic erosion. *Annual Review of Earth and Planetary Sciences*, *34*(1), 419–466. https://doi.org/10.1146/annurev.earth.34.031405.125202

Reiners, P. W., Ehlers, T. A., Mitchell, S. G., & Montgomery, D. R. (2003). Coupled spatial variations in precipitation and long-term erosion rates across the Washington Cascades. *Nature*, *426*, 645–647. https://doi.org/10.1038/nature02111

Reiners, P. W., Farley, K. A., & Hickes, H. J. (2002). He diffusion and (U–Th)/He thermochronometry of zircon: Initial results from Fish Canyon Tuff and Gold Butte. *Tectonophysics*, *349*(1–4), 297–308. https://doi.org/10.1016/S0040-1951(02)00058-6

Robert, X., van der Beek, P., Braun, J., Perry, C., & Mugnier, J.-L. (2011). Control of detachment geometry on lateral variations in exhumation rates in the Himalaya: Insights from low-temperature thermochronology and numerical modeling. *Journal of Geophsical Research*, *116*, B05202. https://doi.org/10.1029/2010JB007893

Robinson, D. M., DeCelles, P. G., Patchett, P. J., & Garzione, C. N. (2001). The kinematic evolution of the Nepalese Himalaya interpreted from Nd isotopes. *Earth and Planetary Science Letters*, *192*(4), 507–521. https://doi.org/10.1016/S0012-821X(01)00451-4

Schelling, D., & Arita, K. (1991). Thrust tectonics, crustal shortening, and the structure of the far-eastern Nepal Himalaya. *Tectonics*, *10*, 851–862. https://doi.org/10.1029/91TC01011

Scherler, D., Bookhagen, B., & Strecker, M. R. (2014). Tectonic control on ^{10}Be-derived erosion rates in the Garhwal Himalaya, India. *Journal of Geophysical Research*, *119*, 83–105. https://doi.org/10.1002/2013JF002955

Schlup, M. (2003). Exhumation history of the western Himalaya: The Rupsha–Lahul–Kullu geochronological transect (NW India), PhD thesis, University of Lausanne (p. 173).

Schlup, M., Steck, A., Carter, A., Cosca, M., Epard, J.-L., & Hunziker, J. (2011). Exhumation history of the NW Indian Himalaya revealed by fission track and 40Ar/39Ar ages. *Journal of Asian Earth Sciences*, *40*, 344–350. https://doi.org/10.1016/j.jseaes.2010.06.008

Singh, R., Prasath, R. A., Paul, A., & Kumar, N. (2018). Earthquake swarm of Himachal Pradesh in northwest Himalaya and its seismotectonic implications. *Physics of the Earth and Planetary Interiors*, *275*, 44–55. https://doi.org/10.1016/j.pepi.2018.01.002

Sobel, E. R., & Seward, D. (2010). Influence of etching conditions on apatite fission-track etch pit diameter. *Chemical Geology*, *271*(1–2), 59–69. https://doi.org/10.1016/j.chemgeo.2009.12.012

Sobel, E. R., & Strecker, M. R. (2003). Uplift, exhumation and precipitation: Tectonic and climatic control of Late Cenozoic landscape evolution in the northern Sierras Pampeanas, Argentina. *Basin Research*, *15*(4), 431–451. https://doi.org/10.1038/35069099

Srivastava, P., & Mitra, G. (1994). Thrust geometries and deep structure of the outer and lesser Himalaya, Kumaon and Garhwal (India): Implications for evolution of the Himalayan fold-and-thrust belt. *Tectonics*, *13*, 89–109. https://doi.org/10.1029/93TC01130

Steck, A. (2003). Geology of the NW Indian Himalaya. *Eclogae Geologicae Helvetiae*, *96*(2), 147–U13. https://doi.org/10.1007/s00015-003-1091-4

Stevens, V. L., & Avouac, J. P. (2015). Interseismic coupling on the Main Himalayan Thrust. *Geophysical Research Letters*, *42*, 5828–5837. https://doi.org/10.1002/2015GL064845

Stübner, K., Grujic, D., Dunkl, I., Thiede, R., & Eugster, P. (2018). Pliocene episodic exhumation and the significance of the Munsiari thrust in the northwestern Himalaya. *Earth and Planetary Science Letters*, *481*, 273–283. https://doi.org/10.1016/j.epsl.2017.10.036

Stübner, K., Grujic, D., Parrish, R. R., Roberts, N. M. W., Kronz, A., Wooden, J., & Ahmad, T. (2014). Monazite geochronology unravels the timing of crustal thickening in NW Himalaya. *Lithos*, *210–211*, 111–128. https://doi.org/10.1016/j.lithos.2014.09.024

Stübner, K., Warren, C., Ratschbacher, L., Sperner, B., Kleeberg, R., Pfänder, J., & Grujic, D. (2017). Anomalously old biotite ^{40}Ar/^{39}Ar ages in the NW Himalaya. *Lithosphere*, *9*(3), 366–383. https://doi.org/10.1130/L586.1

Styron, R. H., Taylor, M. H., & Murphy, M. A. (2011). Oblique convergence, arc-parallel extension, and the role of strike-slip faulting in the High Himalaya. *Geosphere*, *7*(2), 582–596. https://doi.org/10.1130/GES00606.S1

Thakur, V. C., Joshi, M., Sahoo, D., & Suresh, N. (2014). Partitioning of convergence in Northwest Sub-Himalaya: Estimation of late Quaternary uplift and convergence rates across the Kangra re-entrant, North India. *International Journal of Earth Sciences*, *103*, 1037–1056. https://doi.org/10.1007/s00531-014-1016-7

Thiede, R., Arrowsmith, J., & Bookhagen, B. (2005). From tectonically to erosionally controlled development of the Himalayan orogen. *Geology*, *33*, 689–692. https://doi.org/10.1130/G21483AR.1

Thiede, R., Bookhagen, B., & Arrowsmith, J. (2004). Climatic control on rapid exhumation along the southern Himalayan front. *Earth and Planetary Science Letters*, *222*(3–4). https://doi.org/10.1016/j.epsl.2004.03.015

Thiede, R., Robert, X., Stübner, K., Dey, S., & Faruhn, J. (2017). Sustained out-of-sequence shortening along a tectonically active segment of the Main Boundary thrust: The Dhauladhar Range in the northwestern Himalaya. *Lithosphere*, *9*(5), 715–725. https://doi.org/10.1130/L630.1

Thiede, R. C., Arrowsmith, J. R., Bookhagen, B., McWilliams, M., Sobel, E. R., & Strecker, M. R. (2006). Dome formation and extension in the Tethyan Himalaya, Leo Pargil, northwest India. *Geological Society of America Bulletin*, *118*(5/6), 635–650. https://doi.org/10.1130/B25872.1

Thiede, R. C., & Ehlers, T. A. (2013). Large spatial and temporal variations in Himalayan denudation. *Earth and Planetary Science Letters*, *371–372*, 278–293. https://doi.org/10.1016/j.epsl.2013.03.004

Thiede, R. C., Ehlers, T. A., Bookhagen, B., & Strecker, M. R. (2009). Erosional variability along the northwest Himalaya. *Journal of Geophysical Research*, *114*, F01015. https://doi.org/10.1029/2008JF001010

Valdiya, K. S. (1980). The two intracrustal boundary thrusts of the Himalaya. *Tectonophysics*, *66*(4), 323–348. https://doi.org/10.1016/0040-1951(80)90248-6

Valdiya, K. S. (1995). Proterozoic sedimentation and Pan-African geodynamic development in the Himalaya. *Precambrian Research*, *74*(1–2), 35–55. https://doi.org/10.1016/0301-9268(95)00004-O

Vannay, J.-C., & Grasemann, B. (2001). Himalayan inverted metamorphism and syn-convergence extension as a consequence of a general shear extrusion. *Geological Magazine*, *138*(3), 253–276. https://doi.org/10.1017/S0016756801005313

Vannay, J.-C., Grasemann, B., Meinert, R., Carter, F. W. A., Baudraz, V., & Cosca, M. (2004). Miocene to Holocene exhumation of metamorphic crustal wedges in the NW Himalaya: Evidence for tectonic extrusion coupled to fluvial erosion. *Tectonics*, *23*, TC1014. https://doi.org/10.1029/2002TC001429

Webb, A., Yin, A., Harrison, T. M., Célérier, J., Gehrels, G., Manning, C. E., & Grove, M. (2011). Cenozoic tectonic history of the Himachal Himalaya (northwestern India) and its constraints on the formation mechanism of the Himalayan orogen. *Geosphere*, *7*(4), 1013–1061. https://doi.org/10.1130/GES00627.1

Webb, A. A. G. (2013). Preliminary balanced palinspastic reconstruction of Cenozoic deformation across the Himachal Himalaya (northwestern India). *Geosphere*, *9*, 572–587. https://doi.org/10.1130/GES00787

Webb, A. A. G., Yin, A., Harrison, T. M., Celerier, J., & Burgess, W. P. (2007). The leading edge of the Greater Himalayan Crystalline complex revealed in the NW Indian Himalaya: Implications for the evolution of the Himalayan orogen. *Geology*, *35*(10), 955–958. https://doi.org/10.1130/G23931A.1

Whipp, D. M. Jr., Beaumont, C., & Braun, J. (2014). Feeding the "aneurysm": Orogen-parallel mass transport into Nanga Parbat and the western Himalayan syntaxis. *Journal of Geophysical Research: Solid Earth*, *119*, 5077–5096. https://doi.org/10.1002/2013JB010929

Whipple, K. X., Shirzaei, M., Hodges, K. V., & Arrowsmith, J. R. (2016). Active shortening within the Himalayan orogenic wedge implied by the 2015 Gorkha earthquake. *Nature Geoscience*, *9*(9), 711–716. https://doi.org/10.1038/ngeo2797

Willett, S. D. (1999). Orogeny and orography: The effects of erosion on the structure of mountain belts. *Journal of Geophysical Research*, *104*, 28,957–28,981. https://doi.org/10.1029/1999JB900248

Wobus, C., Heimsath, A., Whipple, K., & Hodges, K. (2005). Active out-of-sequence thrust faulting in the central Nepalese Himalaya. *Nature*, *434*, 1008–1011. https://doi.org/10.1038/nature03499

Wobus, C. W., Whipple, K. X., & Hodges, K. V. (2006). Neotectonics of the central Nepalese Himalaya: Constraints from geomorphology, detrital $^{40}Ar/^{39}Ar$ thermochronology, and thermal modeling. *Tectonics*, *25*, TC4011. https://doi.org/10.1038/366557a0

Wolf, R. A., Farley, K. A., & Kass, D. M. (1998). Modeling of the temperature sensitivity of the apatite (U–Th)/He thermochronometer. *Chemical Geology*, *148*(1–2), 105–114. https://doi.org/10.1016/S0009-2541(98)00024-2

Yin, A. (2006). Cenozoic tectonic evolution of the Himalayan orogen as constrained by along-strike variation of structural geometry, exhumation history, and foreland sedimentation. *Earth Science Reviews*, *76*(1–2), 1–131. https://doi.org/10.1016/j.earscirev.2005.05.004